Received: 18 October 2021 | Revised: 1 January 2022 | Accepted: 2 January 2022

DOI: 10.1002/jbio.202100323

JOURNAL OF BIOPHOTONICS

RESEARCH ARTICLE

Three dimensional confocal photoacoustic dermoscopy with an autofocusing sono-opto probe

Haigang Ma[1,2*] | **Zhiyang Wang**[3] | **Chao Zuo**[1] | **Qinghua Huang**[4*]

[1]Smart Computational Imaging (SCI) Laboratory, Nanjing University of Science and Technology, Nanjing, China

[2]Shenzhen Research Institute of Northwestern Polytechnical University, Shenzhen, China

[3]MOE Key Laboratory of Laser Life Science and Institute of Laser Life Science, College of Biophotonics, South China Normal University, Guangzhou, China

[4]School of Artificial Intelligence, Optics and Electronics (iOPEN), Northwestern Polytechnical University, Xi'an, China

***Correspondence**
Haigang Ma, Smart Computational Imaging (SCI) Laboratory, Nanjing University of Science and Technology, Nanjing 210094, China
Email: hsmhgang@163.com
Qinghua Huang, School of Artificial Intelligence, Optics and Electronics (iOPEN), Northwestern Polytechnical University, Xi'an 710072, China.
Email: qhhuang@nwpu.edu.cn

Funding information
Fundamental Research Funds for the Central Universities, Grant/Award Number: 31020200QD040; Guangdong Basic and Applied Basic Research Foundation, Grant/Award Number: 2020A1515110758; National Natural Science Foundation of China under Grants, Grant/Award Number: 62071382; Shaanxi Provincial Foundation for Distinguished Young Scholars under Grant, Grant/Award Number: 2019JC-13

Abstract

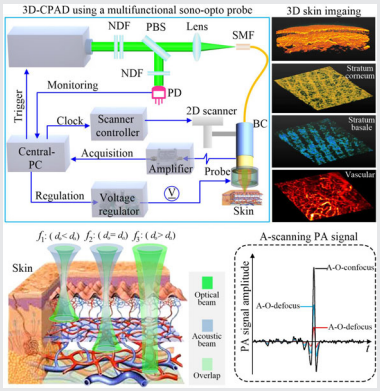

Photoacoustic dermoscopy (PAD) is uniquely positioned for the diagnosis and assessment of dermatological conditions because of its ability to visualize optical absorption contrast in vivo in three dimensions. In this Letter, we developed a 3D confocal PAD (3D-CPAD) equipped with an autofocusing sono-opto probe to facilitate the reconstruction of high-spatial-resolution imaging of skin with multilaminate structures in depth direction. The autofocusing sono-opto probe integrated a 10-mm electrowetting-based varifocal lens to automatically control the acoustic and optical confocal length, and an annular ultrasonic detector with a mid-frequency of ~32.8 MHz is coaxially configured for receiving photoacoustic signals. Using this sono-opto probe, the acoustic and optical confocal length-shifting range from ~7 to 43 mm with high image contrast and spatial resolution in the 3D image reconstruction. Autofocusing property tests and 3D human skin in vivo imaging were carried out to demonstrate the imaging capability of the 3D-CPAD for potential clinical foreground in noninvasive biopsies of skin disease.

1 | INTRODUCTION

Photoacoustic dermoscopy (PAD), an important embranchment of optical absorption–based photoacoustic microscopy (PAM), can be used to acquire high-spatial-resolution imaging of skin tissue with high contrast based on its strong optical absorption and deep acoustic penetration [1–3] and allow functional and structural information via the visualization of skin structures in vivo [4, 5]. Over the recent years, lots of integrated PADs have been developed for the diagnosis of skin diseases such as melanoma [6, 7], port-wine stains [8, 9], psoriasis [10], café au lait spots [11], pigmented nevus [12], scar [13] and human cuticle microvasculature [14, 15] imaging. Several teams developed sono-opto probes for skin imaging without optically focused beam

[16–18], but the resolution and sensitivity were subject to the bandwidth, mid-frequency and the focal spot size of ultrasonic detectors. In order to enhance resolution, some research groups obtained high-resolution skin imaging by a union of a single-mode optical fiber and large numerical aperture optical lens [13, 19–23] but sacrificing skin imaging depth. However, in clinical applications, the human skin with multilaminate structures brings about the out-of-focus scanning of the imaging probe with a single focal length that only can own a narrow focal region. Then, the image contrast and spatial resolution drop rapidly along with the acoustic or optical focus that is far from the target area, which ultimately leads to the imperfection of fine skin imaging.

Therefore, the automatically axial confocal scanning of the sono-opto probe is requested by reason of the worsening of sensitivity and resolution in the out-of-focus location in most PADs [24, 25]. This is especially important for 3D skin imaging that ranges from microns to millimeters with multilaminate structures. Mechanical driver can be used to enlarge the range of focal region of PAMs by moving the optical lens or acoustic detector using a motor or piezoelectric driven microdisplacement platform; nevertheless, the automatically confocal scan of the optical lens and acoustic detector is difficult to obtain in depth direction, and the varifocal speed of the confocus is restricted by the natural inertia of these mechanical devices [26, 27]. To obtain a fast inertialess scanning, an extended depth-of-field lens has been used in PAM, but the PAM is limited by that the optical or acoustic energy is difficult to be evenly distributed in the depth direction [28]. Besides, optical or acoustic fast-focus-depth-scanning schemes have been reported for enlarging the range of focal region of PAMs by varifocal lens [29–31], annular array detectors [31, 32] and multiple sono-opto detectors [24, 33]. In such cases, the limitation of those existing PADs is only one scheme that the acoustic or optical focusing technology is typically adopted, which maybe not enough to meet the need of a large range of confocal region. Meanwhile, fast-confocus-depth-scanning schemes have not been reported in PAD for purpose of acquiring high-resolution 3D skin images in vivo.

In this paper, so as to apply PAD for 3D skin imaging, we report our implementation of an autofocusing sono-opto probe with an electrowetting-based liquid lens, which facilitates acoustic and optical confocus depth scanning over a large depth region. The core components of the probe is a polyvinylidene fluoride (PVDF, which has an acoustic impedance close to the human skin and a high-piezoelectric-voltage coefficients but a low-piezoelectric coefficients; therefore, it obtains advantages in high reception sensitivity for photoacoustic [PA] imaging) detector and an electrowetting-based varifocal lens, which can obtain a confocal coaxial structure of acoustic detection and optical excitation so as to adjust the confocal lengths of the PAD by the supplied voltage values and automatic continuous regulating, and it has been designed and manufactured in our previous PAM [34]. However, because there is no automatic feedback adjustment system in the previous PAM, the sono-opto probe can only scan horizontally at a fixed point of the axial direction during PA imaging so that the PAM is difficult to obtain high-resolution 3D skin imaging with multilayered structures. Here, the automatic focusing technology is developed for the 3D-CPAD, and hence, the sono-opto probe can obtain dynamic confocusing and track the boundary of skin surface based on the PA signal feedback in real time. Subsequent experiments exhibited the progress of 3D confocal PAD (3D-CPAD) for skin imaging with multilayered structures at different depths. Compared with the previous PADs, the 3D-CPAD's main superiority is troubleshooting that the image contrast and spatial resolution deteriorate rapidly owing to the out-of-focus scanning of the sono-opto probe in skin with multilayered structures.

2 | MATERIAL AND METHODS

The schematic of the 3D-CPAD system is shown in Figure 1A, which mainly consists of a 532-nm laser, an autofocusing sono-opto probe, a low-noise amplifier, a 2D scanner and a central personal computer (PC) system for timing control, data acquisition and image reconstruction. The pulsed laser (Model DTL-314QT, Russia) has a maximum repetition rate of 10 kHz and a ~ 4 ns pulse width, which is used as the optical excitation source. The laser beam is focused into a pinhole (20 μm) by an optical lens (LA1222, Thorlabs) for the purpose of spatial filtering, collimated by another same optical lens and then coupled into the single-mode fiber by a fiber port (PAF-X-7-A, Thorlabs). Ultimately, the sono-opto probe is used for optical excitation and acoustic detection by dynamic confocusing and driven mechanically by a 2D scanner (LS2-0830, Guangzhou Jiancheng Photoelectric Co., LTD, China) when the horizontal scanning is performed. A beam splitter was used to reflect around 1% of the laser energy in the optical path, and then, the energy is collected to monitor the variation of the laser power by a photodiode. Meantime, the electrical signal output by the photodiode is used to trigger the central PC system. The central PC system is also used to control the synchronization of the motor scanning, data acquisition and image reconstruction. After PA signals received by the PVDF detector are amplified by a 50-dB low-noise amplifier

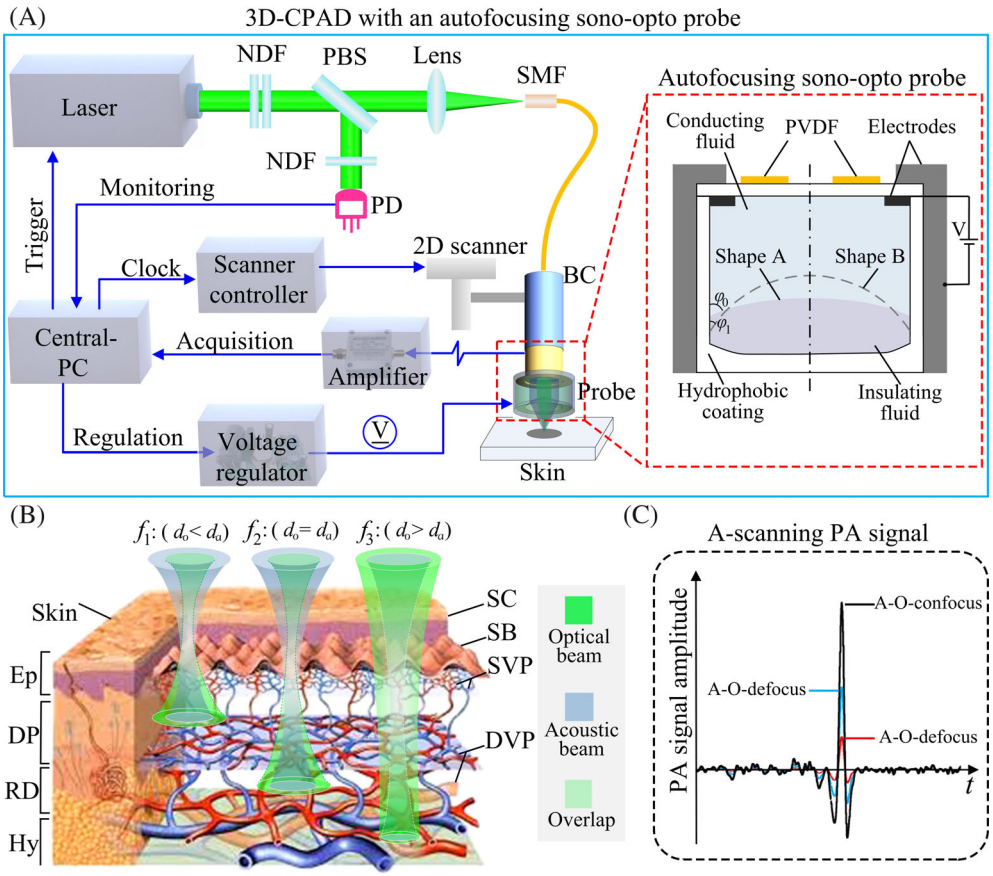

FIGURE 1 3D confocal photoacoustic dermoscopy (3D-CPAD) using an autofocusing sono-opto probe. A, Schematic diagram of the 3D-CPAD. BC, Beam collimator; NDF, neutral-density filters; PBS, polarizing beam splitter; PD, photodiode; PVDF, polyvinylidene fluoride; SMF, single-mode fiber. B, Schematic of light illumination and photoacoustic (PA) signal generation by Chinese people's skin for the autofocusing mode. d_a, The diameter of the acoustic focal spot; d_o, the diameter of the optical focal spot; DP, Dermal papillae; DVP, Deep vascular plexus; Ep, epidermis; f, the focal length; Hy, hypodermis; RD, reticular dermis; SB, stratum basale; SC, stratum corneum; SVP, superficial vascular plexus. C, Principle of generating PA signals for the different acoustic and optical configurations. A-O, acoustic-optical

(AU-1291, MITEQ), they are filtered by a band-pass filter (10 KHz-100 MHz) and ultimately digitized by a high-speed data acquisition card (M3i.4121, SPECTRUM, Germany) at a sampling rate of 250 MHz and stored in the central PC system. The recorded PA signals are processed by a wavelet domain denoising, and the user-defined programs of MATLAB (R2016a, Math Works) and LABVIEW (National Instruments) are used for image reconstructions. Figure 1B displays optical and acoustic focuses in skin tissue at different depths under the situation of the autofocusing sono-opto probe, so the 3D-CPAD can easily switch between optical resolution (OR) mode and acoustic resolution (AR) mode. For instance, the focusing state of the radiation laser at the skin depth of ~1 mm can be considered as an OR-PAD mode (Figure 1B: f_1). On the contrary, when focusing state of the 3D-CPAD is located deep inside the skin tissue, the optical focus is scattered, but the acoustic beam remains well focused, which can turn into an AR-PAD mode (Figure 1B: f_3) [26]. In such a case, with the autofocusing sono-opto probe, switchable scanning can be carried out by OR-PAD mode obtained in the skin depth of ~1 mm, followed by a slow transition to AR-PAD mode in deeper skin depth. Figure 1B,C displays the principle of 3D-CPAD. The PA signal amplitudes excited by the same laser energy between the acoustic/optical focus converging and focusing are significantly different, as the PA signal amplitude is related to the confocal area of the probe. As a result, the adjustment tendency of confocal position of the probe can be predicted by the PA signal amplitude of the 3D-CPAD. Simultaneously, the focal length can be calculated by the time-domain information of PA signals. That is, for the autofocusing mode of the 3D-CPAD, the direct voltage of varifocal lens was driven from the maximum to the minimum per A-line, and the confocal length is automatically adjusted based on the maximal PA signal amplitude.

The adjustable function of this electrowetting-based varifocal lens is achieved by the supplied electrical signal

controlling the curvature radius of the interface of two immiscible liquids. The acoustic and optical beams can permeate through the varifocal lens with the same angle of refraction, which can achieve a confocal coaxial structure of acoustic detection and optical excitation. In this work, it is easy to obtain optical and acoustic confocus by the NaCl solution (22%) as the conducting solution and a mixture of glycerol and silicone oil (mass ratio for glycerol and silicone oil is ~57:43) as the insulating liquid (volume ratio for conducting and insulating liquids is ~17:3). The densities of both the NaCl solution and the mixture liquids are about 1.145 g/cm^3. Therefore, the acoustic and optical confocal length of the varifocal lens can be adjusted flexibly by successively varying the supplied electrical signal. Owing to the difference of refractive index between the NaCl solution (1.37) and the mixed liquids (1.46) of glycerol and silicone oil, it enables the varifocal lens to focus acoustic and optical beams. The acoustic impedances of 22% NaCl and mixture were 1.61 and 2.54 MRayl, respectively, which had less acoustic attenuation. The relationship between supplied electrical signal (U) and radius of the interface curvature of two immiscible liquids for varifocal lens can be calculated by [35, 36]:

$$r = -a/\left[\cos\varphi_0 + \varepsilon_0\varepsilon_r U^2/(2\gamma d)\right]. \quad (1)$$

Here, a is the inner radius of hydrophobic coating material, φ_0 is the natural contact angle at the voltage of 0 V, ε_0 is the absolute permittivity of free space and ε_r is the relative permittivity, γ is the tension coefficient of the interface of two immiscible liquids, and d is the thickness of skirt board of hydrophobic coating material. For the sono-opto probe, a drop of about 0.15 ml of the mixture of glycerol and silicone oil as the insulating liquid and a drop of about 0.85 ml of 22% NaCl solution as the conducting solution are injected with a syringe before closing.

3 | RESULTS

Setting this varifocal lens on its diverging or focusing mode can be acquired by deliberately selecting the operating fluids inside the cylinder lens, which by principle is the approach to electrowetting-based optical varifocal lens. For 3D-CPAD, the confocusing performance of the sono-opto probe is the important quality, which directly affects the image reconstruction. To obtain an optical intensity distribution, the transparent gelatin phantom was used as a medium for optics propagation, and then, the axial distribution of optical intensity was recorded by a CCD camera and the horizontal distribution of focal position was measured by a spot analyzer. Meantime, a pulser/receiver (5073PR, Olympus) was used to excite the probe to produce ultrasonic waves, and a hydrophone (HPM02, Precision Acoustics Ltd.) with a circular sensing area of 0.2 mm in diameter was used to scan axially and laterally when receiving the ultrasonic waves from the PVDF detector. The relationship between the supplied electrical signal (applied voltage) and the curvature of the interface curvature of two immiscible liquids is characterized and shown in Figure 2A. A custom voltage regulator was used to control the confocal length of the probe by delivering an adjustable direct voltage output from 0 to 60 V, with an adjusting precision of 1 mV. The maximum varifocal range of the probe from 0 to 60 V was measured, which was ~36 mm, and had a ~ 5 μm accuracy of focusing continuously as shown in Figure 2B. The pulse-echo response of the PVDF detector at 6.5 mm confocal length (black line) is shown in Figure 2C, and the red line is its Hilbert-transformed envelope. The axial resolution of the 3D-CPAD with confocal length of 6.5 mm was measured to be ~44.6 μm by the full width at half maximum (FWHM) of the envelope. Also, by the amplitude–frequency response of the detector, the central frequency and fractional bandwidth can be determined, which were ~ 32.8 and ~ 45.4 MHz at −6 dB, respectively, as shown in Figure 2D. In the PAD, we used a laser with a repetition rate of 5 KHz, so the image uniform acquisition time is approximately 0.2 second for a ~ 5 mm B-Scan PA imaging area with a scanning step of ~5 μm, and the response time of the sono-opto probe is ~50 ms.

In the 3D-CPAD, the repetition rate of the pulsed laser is 5 KHz, so the mean acquisition time of data is ~0.2 second for a ~ 5 mm B-Scan imaging range, with a scanning interval of ~5 μm. To remove the influence of the inertia of the varifocal lens, the acceleration and deceleration processes of the probe during image reconstruction were eliminated; that is, the probe was always operated on the uniform speed stage. Figure 3A shows the experimental result about diameters of the optical and acoustic focal spots as functions of the applied voltage. As the applied voltage is increased, the interface deformities of two immiscible liquids become more obvious so that the radius of curvature of the interface is decreasing, which eventually causes the focal length to decrease, according to Equation (1). Owing to the performance of varifocal lens is affected by the f-number, the resolution of 3D-CPAD can be changed as the variation of confocus. Figure 3B shows the distributions of optical intensity and acoustic pressure when the voltage of 50 V is applied. Sure enough, the optical intensity and acoustic pressure were highly converged when a voltage was applied. The FWHM of the line spread function was

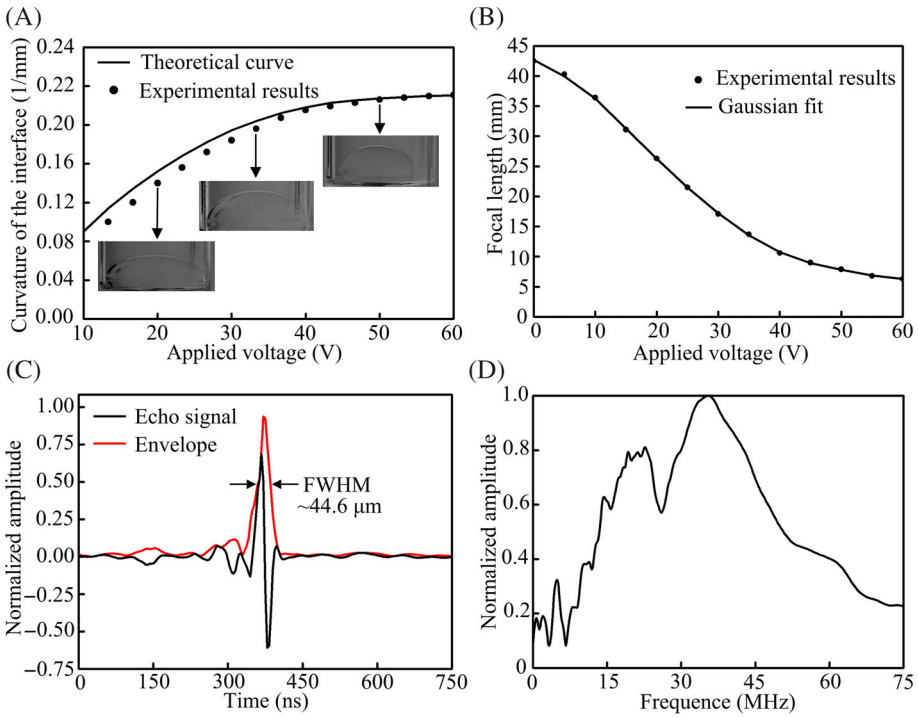

FIGURE 2 Acoustic and optical features of the autofocusing sono-opto probe. A, Curvature of the interface of two transparent immiscible liquids as a function of the applied voltage. B, The relationship between confocal length and applied voltage. C, The pulse response of PVDF detector at the confocal position. D, Amplitude frequency response of the probe. FWHM, Full width at half maximum; PVDF, polyvinylidene fluoride

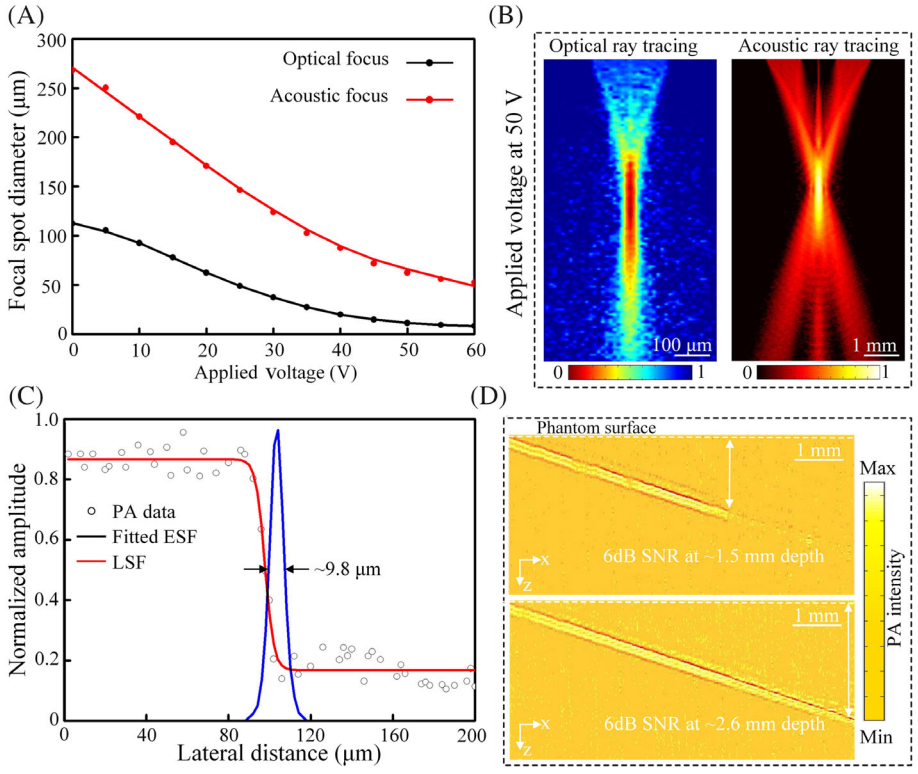

FIGURE 3 Resolution and penetration depths of the 3D-CPAD system. A, Diameters of the optical and acoustic focal spots as functions of the applied voltage. B, Distributions of optical intensity and acoustic pressure when the applied voltage is 50 V. C, Edge spread function (ESF) extracted from the PAD image of a sharp-edged surgical blade obtained by the 3D-CPAD and line spread function (LSF) acquired by processing the derivative of the ESF. D, Single B-scan images of a black hair with a diameter of 50 μm obliquely inserted into a human skin tissue–mimicking phantom were acquired by the imaging system for fixed-focus and autofocusing modes, respectively. 3D-CPAD, 3D confocal photoacoustic dermoscopy; PA, photoacoustic; SNR, signal-to-noise ratio

estimated to be ~9.8 μm by a "blade method" when the applied voltage of 50 V [19], as shown in Figure 3C, which represented the lateral resolution of the system under 50 V. To display the imaging depth of 3D-CPAD, a black hair with the diameter of 50 μm obliquely inserted into a human skin tissue–mimicking phantom (the optical absorption coefficient is ~0.01 mm^{-1}, the reduced scattering coefficient is ~1.0 mm^{-1}, and the acoustic impedance is ~1.5 MRayl) was imaged. To conform to the American National Standards Institute safety limit [37], the laser fluence on the surface of the phantom at 532 nm was set to ~10 mJ/cm^2. The autofocusing-

imaging mode of the 3D-CPAD system can image the hair ~2.6 mm below the surface of the phantom with a signal-to-noise ratio (SNR) of 6 dB compared to only ~1.5 mm by a fixed focus-imaging mode of that with the same SNR (Figure 3D). As a result, the 3D-CPAD system with an autofocusing sono-opto probe can penetrate more deeply than the common PAD with a fixed focal probe. And the repeatability of focal change over the voltage applied is very good. In order to avoid the influence of the inertia of the liquids, the acceleration and deceleration processes of the sono-opto probe during PA imaging were eliminated; that is, the probe was always operated on the uniform speed stage.

To investigate the ability of 3D-CPAD for structural visualization of human skin, the optimal 3D imaging was carried out at the palm and opisthenar skins of one author by the autofocusing-imaging mode to vary the depth of the position of confocus with respect to the skin surface as displayed in Figure 4. All the human experiments followed a protocol approved by the Institutional Review Board administered by the Human Research Protection Office at South China Normal University in Guangzhou. Figure 4A showed the reconstructed 3D images for palm and opisthenar skins, and the imaging area is 5 × 5 mm (scan points, 1000 × 500), taking a time of ~2 minutes per PA image. The entire volunteer handling process, including placement of the sono-opto probe on the skin tissue surface, lasted less than 5 minutes. And the imaging depth in the PA images in Figure 4A is about 1.8 mm. Figures 4B-D displayed the 3D images in the direction perpendicular to the skin surface at different depths labeled in Figure 4A. As is shown in Figure 4B, the

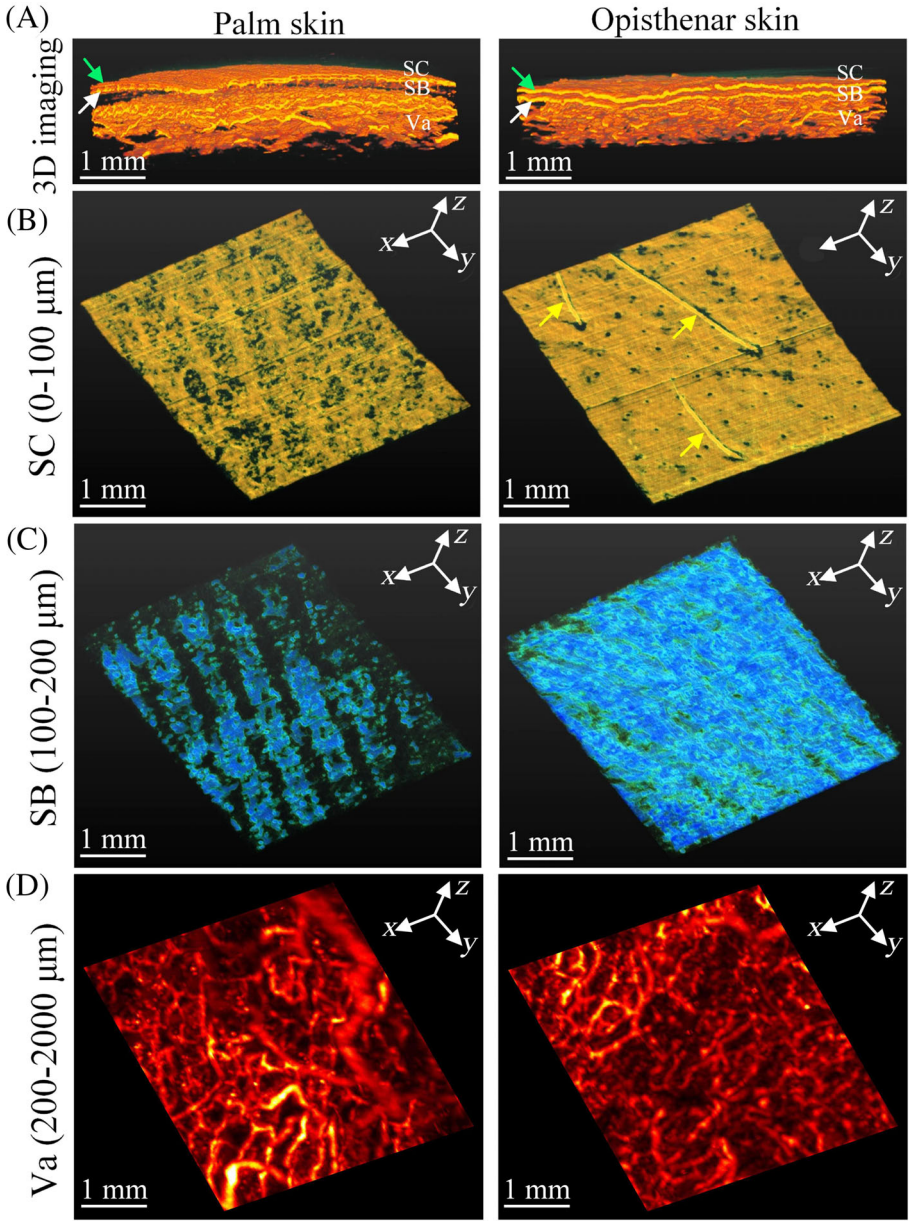

FIGURE 4 Comparison of contrasts by palm and opisthenar skins of one author in vivo using the 3D-CPAD. A, 3D skin PA images of the palm and opisthenar skins. The arrows (green and white) indicate the stratum corneum (SC) and the stratum basale (SB) in the upper part of vascular (Va) network, respectively. B, 3D images of the SC depicting a slice in the depth range of ~0 to 100 μm below the skin surface. The yellow arrows indicate fine hairs on the opisthenar skin. C, 3D images of the SB in the depth range of ~100 to 200 μm below the skin surface. D, 3D images of the Va network below the skin surface in the depth range of ~200 to 2000 μm. 3D-CPAD, 3D confocal photoacoustic dermoscopy; PA, photoacoustic

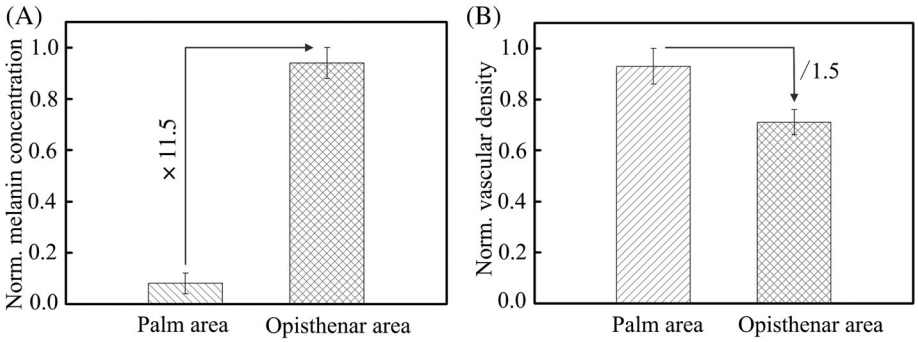

FIGURE 5 The difference between the PA images of palm and opisthenar skins. A, The normalized melanin concentration of the epidermal layer. B, The normalized vascular density of dermal layer. PA, Photoacoustic

stratum corneum (SC) within palm and opisthenar skins is usually located at a depth of less than 100 μm, and the SC within palm skin can be regarded as a skin texture character with microarchitecture as small as 20 μm, and fine hairs and sweat pores in opisthenar skin can be presented, which displays that the traits of the even skin surface are significant difference between palm and opisthenar skins. The 3D images of the stratum basale (SB) are displayed in Figure 4C. As depicted, below the SB is the area in which the skin pigment (mainly melanin) is situated in palm and opisthenar skins. Meantime, the results indicate that the skin pigment content of palm and opisthenar skins is the significant variation between palm and opisthenar skins. Under SB, the vascular network that belongs to both the superficial vascular plexus of the dermis and the deeper vascular plexus of hypodermis can be presented as displayed in Figure 4D. The vascular network between depths of 200 and 2000 μm relative to the skin surface is shown in Figure 4D, whose diameters range from ~20 to 300 μm, and the palm skin of the author has more blood volume and more intricacy morphophysical structures for this layer. As shown in Figure 5, the normalized melanin concentration of the epidermal layer of the palm skin is significantly smaller than that of the opisthenar skin. Meanwhile, the normalized vascular density of dermal layer of opisthenar skin is significantly smaller than that of the palm skin.

4 | DISCUSSION AND CONCLUSIONS

In conclusion, we developed a 3D-CPAD using an autofocusing sono-opto probe that facilitates a confocal dynamic adjustment range up to several centimeters. The sono-opto probe is mainly made of an electrowetting-based varifocal lens and a PVDF detector. The varifocal lens composed of two transparent immiscible liquids that are used as acoustic-optical varifocal lenses. Using the autofocus scanning mode, the probe enables 3D-CPAD to obtain 3D skin imaging with high spatial resolution and sensitivity. Thus, unlike conventional PAD that operates at a single acoustic or optical focusing scan, the 3D-CPAD, which accelerates acoustic and optical isochronous confocal scanning within a large depth, can effectively resolve the skins of image contrast and spatial resolution deterioration when the target is out of focus. As such, this instrument has a broad prospect for the clinical diagnosis of skin diseases and facilitating the progress of the rapid noninvasive 3D skin imaging in vivo.

ACKNOWLEDGMENTS

This research was supported by the Guangdong Basic and Applied Basic Research Foundation (2020A1515110758), Fundamental Research Funds for the Central Universities (31020200QD040), National Natural Science Foundation of China under Grant (62071382), and Shaanxi Provincial Foundation for Distinguished Young Scholars under Grant (2019JC-13).

CONFLICT OF INTEREST

The authors declare that there are no conflicts of interest.

DATA AVAILABILITY STATEMENT

The data that support the findings of this study are available from the corresponding author upon reasonable request.

ORCID

Haigang Ma https://orcid.org/0000-0001-7936-4971
Zhiyang Wang https://orcid.org/0000-0002-9262-2899
Chao Zuo https://orcid.org/0000-0002-1461-0032

REFERENCES

[1] X. L. Dean-Ben, D. Razansky, *Exp. Dermatol.* **2021**, *30*, 1598.
[2] H. F. Zhang, K. I. Maslov, L. V. Wang, *J. Biomed. Opt.* **2009**, *14*, 024050.
[3] I. Steinberg, D. M. Hulandad, O. Vermesh, H. E. Frostig, W. S. Tummers, S. S. Gambhir, *Photoacoustics* **2019**, *14*, 77.
[4] A. B. E. Attia, G. Balasundaram, M. Moothanchery, U. S. Dinish, R. Bi, V. Ntziachristos, M. Olivo, *Photoacoustics* **2019**, *16*, 100144.

[5] S. Cho, J. Baik, R. Managuli, C. Kim, *Photoacoustics* **2020**, *18*, 100168.
[6] P. Hai, Y. Qu, Y. Li, L. Zhu, L. Shmuylovich, L. A. Cornelius, L. V. Wang, *J. Biomed. Opt.* **2020**, *25*, 036002.
[7] J. Kim, Y. H. Kim, B. Park, H.-M. Seo, C. H. Bang, G. S. Park, Y. M. Park, J. W. Rhie, J. H. Lee, C. Kim, *Br. J. Dermatol.* **2018**, *179*, 780.
[8] D. Xu, S. Yang, Y. Wang, Y. Gu, D. Xing, *Biomed. Opt. Express* **2016**, *7*, 2095.
[9] H. Zhang, G. Zhang, Y. Zhang, L. Wen, M. Zhang, J. Pan, P. Wang, X. Wang, Q. Cheng, X. Wang, *J. Am. Acad. Dermatol.* **2021**, *85*, 1613.
[10] J. Aguirre, M. Schwarz, N. Garzorz, M. Omar, A. Buehler, K. Eyerich, V. Ntziachristos, *Nat. Biomed. Eng.* **2017**, *1*, 68.
[11] H. Ma, Z. Cheng, Z. Wang, Y. Gu, T. Zhang, H. Qiu, S. Yang, *Appl. Phys. Lett.* **2018**, *113*, 083704.
[12] C. P. Favazza, L. V. Wang, O. W. Jassim, L. A. Cornelius, *J. Biomed. Opt.* **2011**, *16*, 016015.
[13] Z. Cheng, H. Ma, Z. Wang, S. Yang, *Front. Optoelectron.* **2020**, *13*, 307.
[14] J. Ahn, J. Y. Kim, W. Choi, C. Kim, *Photoacoustics* **2021**, *23*, 100282.
[15] H.-C. Hsu, L. Wang, L. V. Wang, *J. Biomed. Opt.* **2016**, *21*, 056004.
[16] M. Schwarz, D. Soliman, M. Omar, A. Buehler, S. V. Ovsepian, J. Aguirre, V. Ntziachristos, *IEEE Trans. Med. Imaging* **2017**, *36*, 1287.
[17] J. Sun, Q. Zhou, S. Yang, *Opt. Express* **2018**, *26*, 4967.
[18] L. Xi, H. Jiang, *Appl. Phys. Lett.* **2015**, *107*, 063701.
[19] H. Ma, S. Yang, Z. Cheng, D. Xing, *Opt. Lett.* **2017**, *42*, 2342.
[20] A. A. Plumb, N. T. Huynh, J. Guggenheim, E. Zhang, P. Beard, *Eur. Radiol.* **2018**, *28*, 1037.
[21] W. Bost, R. Lemor, M. Fournelle, *IEEE Trans. Med. Imag.* **2014**, *33*, 1900.
[22] H. Ma, K. Xiong, J. Wu, X. Ji, S. Yang, *Appl. Phys. Lett.* **2019**, *114*, 133701.
[23] Z. Wang, F. Yang, Z. Cheng, W. Zhang, K. Xiong, S. Yang, *Nanophotonics* **2021**, *10*, 3359.
[24] Z. Wang, F. Yang, H. Ma, Z. Cheng, S. Yang, *J. Biophotonics* **2020**, *13*, e202000145.
[25] W. Zhang, H. Ma, Z. Cheng, Z. Wang, L. Zhang, S. Yang, *Quant. Imag. Med. Surg.* **2019**, *9*, 807.
[26] H. Ma, Z. Cheng, Z. Wang, W. Zhang, S. Yang, *Appl. Phys. Lett.* **2020**, *116*, 073703.
[27] M. Nasiriavanaki, J. Xia, H. L. Wan, A. Q. Bauer, J. P. Culver, L. V. Wang, *Proc. Natl. Acad. Sci. U. S. A.* **2014**, *111*, 21.
[28] D. Zhang, Z. Wang, Z. Cheng, W. Zhang, F. Yang, S. Yang, *I.E. E.E. Trans. Biomed. Eng.* **2021**, *68*, 3748. https://doi.org/10.1109/TBME.2021.3078729.
[29] B. Li, H. Qin, S. Yang, D. Xing, *Opt. Express.* **2014**, *22*, 20130.
[30] P. Hajireza, A. Forbrich, R. J. Zemp, *Opt. Lett.* **2013**, *38*, 2711.
[31] C. Song, L. Xi, H. Jiang, *Opt. Lett.* **2013**, *38*, 2930.
[32] Z. Liu, C. Tao, X. Liu, *Appl. Phys. Express.* **2019**, *12*, 057001.
[33] Y. Tang, W. Liu, Y. Li, Q. Zhou, J. Yao, *VCIBA* **2018**, *1*(1), 1.
[34] H. Ma, Z. Cheng, Z. Wang, K. Xiong, S. Yang, *Opt. Lett.* **2019**, *44*, 1880.
[35] G. Feng, G. Chu, *Sens. Actuator A Phys.* **2014**, *208*, 130.
[36] R. Peng, J. Chen, C. Zhu, S. Zhuang, *Opt. Express.* **2007**, *15*, 6664.
[37] Laser Institute of America, American National Standard for Safe Use of Lasers ANSI Z136.1-2014, American National Standards Institute, Inc., **2014**.

How to cite this article: H. Ma, Z. Wang, C. Zuo, Q. Huang, *J. Biophotonics* **2022**, e202100323. https://doi.org/10.1002/jbio.202100323